Effect of radiolysis of TODGA on the extraction of TODGA/n-dodecane toward Eu(III): An experimental and DFT study

Hang Zhang[1,2]‡, Yin-Yong Ao[3]‡, Yue Wang[2], Shang-Jie Zhao[1], Jia-Yang Sun[1,2], Mao-Lin Zhai[2], Jiu-Qiang Li[2], Jing Peng[2]*, Hui-Bo Li[1]*

[1] *Department of Radiochemistry, China Institute of Atomic Energy, Beijing 102413, China*

[2] *Beijing National Laboratory for Molecular Sciences, Radiochemistry and Radiation Chemistry Key Laboratory for Fundamental Science, College of Chemistry and Molecular Engineering, Peking University, Beijing 100871, China*

[3] *Institute of Nuclear Physics and Chemistry, China Academy of Engineering Physics, Mianyang 621900, China*

‡ These authors contributed equally to this work.

Corresponding Author, E-mail: jpeng@pku.edu.cn, hb0012@sina.com

Effect of radiolysis of TODGA on the extraction of TODGA/n-dodecane toward Eu(III): An experimental and DFT study

Abstract: N,N,N',N'-Tetraoctyl diglycolamide (TODGA) is one of the most promising extractants tailored for high-level liquid radioactive waste treatment during nuclear fuel reprocessing. The γ-radiolysis of TODGA (0.2 mol/L) in *n*-dodecane (*n*DD) solution with and without pre-equilibrated 3.0 mol/L HNO_3 was investigated using HPLC and UPLC-QTOF-MS and compared with the γ-radiolysis of neat TODGA in this study. With increased absorbed doses, the concentration of TODGA decreased exponentially for the studied systems. Moreover, pre-equilibration with HNO_3 (3.0 mol/L) slightly influenced the γ-radiolysis of TODGA in *n*DD. Seven radiolytic products generated from the rupture of the C – C, C – O, and C – N bonds in TODGA were identified in the studied extraction system. The influence of γ-radiation on TODGA/*n*DD for the extraction of Eu(III) was evaluated using the first combination of extraction experiments and density functional theory (DFT) calculations, in which the complexations of Eu(III) with TODGA and its radiolytic products were systematically compared. Based on the radiolysis kinetic model of TODGA, the slope curve of the distribution ratio of Eu(III) (D_{Eu}) and the absorbed dose, and fluorescence titration analysis, the empirical equation of the absorbed dose and D_{Eu} was obtained successfully. Below 300 kGy, the experimental D_{Eu} agreed well with the obtained empirical equation for TODGA/*n*DD. Conversely, at a high absorbed dose, the experimental D_{Eu} was higher than the theoretical D_{Eu} based on the empirical equation because the radiolytic products of TODGA with similar coordination structures still possessed partial complexation toward Eu(III), which was confirmed by DFT calculations. This work provides a method to predict the extraction distribution ratio of an irradiated extractant system and to understand the complex extraction process.

Keywords TODGA; Radiolytic products; Extraction; Density functional theory; Complexation

1 Introduction

Spent nuclear fuel (SNF) reprocessing generates high-level liquid radioactive waste (HLLW), which is composed of unextracted U and Pu, long-lived fission products (^{129}I, ^{99}Tc, ^{135}Cs, and ^{93}Zr), short-lived fission products (^{90}Sr and ^{137}Cs), minor actinides (MAs) (Np, Am, and Cm), and stable lanthanide isotopes (Eu, Nd, La, Tb, Pr, Gd, Sm, Ce, and Pm)[1–10]. To reduce the radiotoxicity and volume of HLLW and improve resource utilization, partitioning and transmutation strategies have been explored to shorten the half-life of long-lived radioisotopes. However, the transmutation efficiency of MAs is limited by the high thermal neutron capture cross-sections of several lanthanide isotopes owing to competition for available neutrons[11, 12]. Thus, separating MAs from lanthanides (Lns) before transmutation is crucial.

During the liquid–liquid extraction process, N,N,N’,N’-tetraoctyl diglycolamide (TODGA) has proven to be efficient in extracting actinides (Ans) and lanthanides [2, 13–16]. Furthermore, TODGA is a tridentate ligand that shows high distribution ratios for Lns(III)/Ans(III) because the hydrophilic groups exhibit stable metal coordination in the aqueous phase and the hydrophobic groups ensure its solubility in the organic phase[17, 18]. It has been used in some processes, such as the innovative Selective ActiNide EXtraction (i-SANEX) process[19, 20] and the EUROpean Grouped Actinide EXtraction (EURO-GANEX) process[21, 22]. The i-SANEX process was first arranged utilizing an organic solution with TODGA (0.2 mol/L) and 1-octanol (5% v/v) to enable co-extraction of trivalent Lns and Ans from simulated HLLW. At the same time, Pd and Zr were masked by cyclohexane diamine tetraacetic acid (CDTA). Second, the co-extracted Mo and Sr were stripped using 3.0 mol/L HNO_3 aqueous solution with CDTA (0.05 mol/L) and oxalic acid (0.2 mol/L) as scrubbing solvents, followed by a back-extraction step using an aqueous solution containing 2,6-bis(5,6-di(sulfophenyl)-1,2,4-

triazin-3-yl)pyridine (SO_3-Ph-BTP) (1.8×10^{-2} mol/L) in HNO_3 (0.35 mol/L) for selective stripping of Ans(III). The final step was the stripping of Lns(III) using a citrate buffer solution. The experimental results obtained by Wilden et al.[19] demonstrated the effectiveness of this process. In the Ans product fraction, Cm(III) and Am(III) were efficiently stripped (more than 99.8%) and regained within six stages. The purity of the Cm(III) and Am(III) products was found to be very good, with only Ru (0.4%), Sr (0.3%), and Lns(III) (0.1%) contamination. Lns(III) stripping is efficient (more than 99.5%) within only four stages using a stripping solution containing citric acid with a pH of 3. The EURO-GANEX process consists of two cycles. In the first cycle, hydrogenated tetrapropene (TPH) containing N,N-di (2-ethylhexyl) isobutyramide (DEHiBA) (1.0 mol/L) was applied to extract U(VI) selectively. In the second cycle, the extraction of Cm(III), Am(III), Pu(IV), Np(VI), and Lns(III) from the first cycle raffinate was achieved using N,N'-dimethyl-N,N'-dioctyl-2(2-hexyloxyethyl)-malonamide (DMDOHEMA) (0.5 mol/L) and TODGA (0.2 mol/L) in a kerosene diluent, while CDTA (0.055 mol/L) was applied as a masking agent, to prevent the extraction of Zr(IV) and Pd(II). The Sr and Fe were extracted using HNO_3 (0.5 mol/L) from the loaded solvent, and trans-uranium elements (TRU) were back-extracted by applying an aqueous solution containing aceto-hydroxamic acid (AHA) and SO_3-Ph-BTP, while Lns(III) was retained in the organic solution. The EURO-GANEX process was successfully demonstrated by the hot test performed by Malmbeck et al.[23]. Moreover, Pu(IV), Np(VI), Am(III), and Lns(III) were efficiently co-extracted from the raffinate of the EURO-GANEX process during the first cycle; Mo and Zr were also co-extracted, whereas the other fission products were successfully refused. Within six strip stages, 99.91% Np, 99.85% Pu, 99.90% Am, and co-extracted Mo and Zr were well

back-extracted, whereas 99.9% Lns(III) was retained in the organic solution within four strip stages using an aqueous solution containing AHA and SO_3-Ph-BTP.

Previous studies have shown that TODGA provides significantly higher distribution ratios in alkanes such as *n*-dodecane (*n*DD) than in other studied diluents, such as secondary ketones, primary alcohols, and secondary alcohols[24, 25]. The extraction system of TODGA/*n*DD can be applied to separate MAs and Lns from other fission products. Once separated, the extraction of individual elements can be simplified with additional processing, culminating in the separation of MAs from Lns [26–28].

Because the extraction system is exposed to the radioactive environment formed by the radionuclides, its radiation stability is an important factor to be examined before its practical application[29]. In the solvent extraction process, the γ-radiolysis of TODGA is problematic because of the highly radioactive HLLW. Because the loss of TODGA and the radiolytic products of TODGA formed during γ-radiation can adversely affect the extraction performance in the liquid–liquid extraction process toward metal ions, it is essential to measure the γ-radiolysis yield and radiolytic products of TODGA and to study their effects on the performance of extracting metal ions. Radiolysis of TODGA in *n*DD under different conditions has been investigated in some studies [30, 31]. It was found that the magnitude of α-radiolysis of TODGA is lower than that of γ-radiolysis, and they have similar radiolytic products[32]. This is attributed to the fact that the linear energy transference of α particles is higher than that of γ particles, and the radical yield of *n*DD decreases by recombination in α-radiolysis. Although the γ-radiolysis and extraction of TODGA have been investigated, the effect of γ-radiolysis and radiolytic TOGDA products on extraction in the TODGA/*n*DD system has rarely been reported. In addition, if we could predict the extraction performance of the irradiated extractant system using equations, it would be very beneficial and important in controlling the

partition process. To the best of our knowledge, the mathematical correlation between the radiolysis of the extractant and the distribution ratio has seldom been studied.

In this work, because α and γ rays result in similar radiolysis products of TODGA and γ-radiation is easier to carry out in the laboratory, the radiolytic behavior and γ-radiation stability of TODGA in the 0.2 mol/L TODGA/*n*DD system (TODGA/*n*DD) and the 0.2 mol/L TODGA/*n*DD that was pre-equilibrated with 3.0 mol/L HNO_3 system (HNO_3-TODGA/*n*DD) were studied qualitatively and quantitatively. They were also compared with radiolysis of neat TODGA. The content and radiolysis products of TODGA were determined using HPLC and UPLC-QTOF-MS, respectively. Considering the chemical similarity between trivalent lanthanides and minor actinides, and to avoid the dangers of handling radioactive isotopes in standard laboratories, Eu(III) was selected as a model metal ion in our extraction experiment to assess the extraction performance of TODGA/*n*DD after γ-radiation. The density functional theory (DFT) calculation, which can estimate the coordination abilities of TODGA and its radiolytic products, was applied to explain the effect of the radiolytic products on our extraction of Eu(III). For the first time, a combination of theoretical calculations and extraction experiments was used to demonstrate that the radiolytic products maintain partial complexation, which capably explains the extraction behavior of irradiated samples. For the TODGA/nDD system, an in-depth understanding of the effects of γ-irradiation on the extraction behavior was obtained from this study.

2 Experimental

Materials

Sichuan University synthesized TODGA (≥98%); its purity was confirmed by FT-MS (ESI^+) and ^1H NMR (Figure S1 – 2). Moreover, $Eu(NO_3)_3 \cdot 6H_2O$ (99.99%) was obtained from MREDA Technology Co. Ltd. Formic acid, liquid chromatography-mass spectrometry (LC-MS) grade, was purchased from Thermo Fisher Scientific. Methanol (LC-MS grade) was purchased from Honeywell Trading (Shanghai) Co., Ltd. The aqueous dilution was performed using ultrapure water (18.2 MΩ·cm). All other chemicals were of analytical grade, and the chemicals were not further purified.

Gamma irradiation

TODGA and TODGA/*n*DD solutions equilibrated with and without HNO_3 (3.0 mol/L) before γ-radiation were irradiated in the air at room temperature (25 ± 5 °C) using a ^{60}Co source (Department of Applied Chemistry in the College of Chemistry, Peking University, China) with an absorbed dose rate of 6.6 kGy/h, as determined by a Fricke dosimeter.

Quantitative analysis of TODGA after irradiation

An HPLC method with UV detection (SPD-16, Shimadzu, Japan) was used to quantitatively analyze the TODGA concentration in the irradiated samples. Additionally, HPLC was carried out at 25 ± 5 °C using an Agilent HC-C18 liquid chromatography column (5 μm, 4.6 mm × 150 mm) to achieve chromatographic separation with a UV wavelength fixed at 210 nm. The aqueous component was ultrapure water with formic acid (1‰ v/v) (A); the organic component was methanol (B). The elution program in our liquid chromatography was listed hereafter: 0–10 min, 30–100% B; 10–20 min, 100% B; 20–22 min, 100–30% B. The error values in the quantitative analysis experiments were within 5%. The flow rate was 1.0 mL/min, and the injection volume was 20 μL.

Identification and semi-quantification of radiolytic products

Ultra-high pressure liquid chromatography (UPLC) (ACQUITY I-Class, Waters, USA) was carried out using an Agilent HC-C18 liquid chromatography column (5 μm, 4.6 mm × 150 mm) at 40 °C to achieve chromatographic separation. The aqueous component was ultrapure water with formic acid (1‰ v/v) (A), and the organic component was methanol with formic acid (1‰ v/v) (B). The liquid chromatography elution program was listed hereafter: 0–4 min: 30–100% B; 4–13 min: 100% B; 13–13.1 min: 100–30% B; 13.1–15 min: 30% B. The flow rate was 0.8 mL/min with a 1 μL injection volume. The mass-spectrometer conditions of the quadrupole time-of-flight mass spectrometry (QTOF-MS) (Vion IMS QToF, Waters, USA) are listed here: desolvation temperature: 300 °C; source temperature: 120 °C; desolvation gas flow: 800 L/h; capillary voltage: 2.8 kV; cone gas flow: 50 L/h; positive mode. The data were acquired and processed using a Waters UNIFI Scientific Information System with a mass target match tolerance of less than 5 ppm.

Extraction experiment

The TODGA was dissolved with *n*DD to obtain a 0.7 ml organic phase with a concentration of 0.2 mol/L. The $Eu(NO_3)_3 \bullet 6H_2O$ was dissolved in 3.0 mol/L HNO_3 to obtain a 0.7 ml aqueous phase with a concentration of 1000 mg/L. Pre-equilibration of the organic extraction phase with 3.0 mol/L HNO_3 was performed before extraction. A vortex mixer at a speed of 2500 rpm (LPD2500, Leopard Scientific Instrument Co., Ltd, Beijing) was used to perform the extraction experiments at 298 ± 1 K. To achieve complete separation between the two phases, the mixtures were centrifuged for 1 min at 5000 rpm in a centrifuge (TGL-16M, Cence, Hunan). After dilution with ultrapure water, the aqueous phase was detected using an ICP-MS (ELEMENT XR, Thermo Scientific, USA) to estimate the concentration of Eu(III).

The distribution ratio of Eu(III) (D_{Eu}) was calculated using Eq. (1). The phase ratio equals 1:1 in the extraction experiment.

$$D_{Eu} = (C_i - C_f)/C_f \quad (1)$$

where C_f and C_i represent the final and initial Eu (III) concentrations in the diluted aqueous phase, respectively. The extraction had an error rate of less than 5%.

Fluorescence spectra titration

The fluorescence emission spectra of the titration experiments were investigated at 298 ± 1 K in a cuvette cell with a 1 cm path length using a fluorescence spectrophotometer (F7000, Hitachi, Japan). The concentration of TODGA was 0.1 mol/L in acetonitrile and the initial concentration of Eu(III) was 0.001 mol/L in 2.0 mL acetonitrile. Next, 4 μL of TODGA solution was added at a time. The solution was mixed using a vortexer (VORTEX 3, IKA, Germany) for 5 min after the addition of each ligand. The titration experiments used an excitation wavelength of 395 nm; the bandwidth of the excitation and emission was 2.5 nm. The interval was 1 nm and the spectra were recorded between 550 and 700 nm. Single-component spectra of the metal–ligand complexes and metal solvent species were obtained using the HyperSpec program.

Theoretical calculations

DFT calculations incorporating electron correlation effects were performed at the level of B3LYP using the Gaussian 09 package [33–35]. The relativistic effects of Eu atoms were investigated using the quasi-relativistic effective core potentials (RECPs) and associated valence basis sets, which were improved by the Stuttgart and Dresden groups[36–40]. The large-core RECPs used in the structural optimization of Eu(III) contained 52 electrons[39, 40]. All other C, N, O, and H atoms utilized the 6-31G (d) basis set. Geometrical optimization and the electronic calculations of all structures were

first performed at the level of B3LYP/6-31G(d)/RECP under the gas phase conditions. The Gibbs free energy (G_g), entropy (S_g), and enthalpy (H_g) were obtained under the gas phase conditions at 298.15 K using the same theory level. To obtain the Gibbs free energy (G_{aq}), entropy (S_{aq}), and enthalpy (H_{aq}) of the species in the *n*DD phase at 298.15 K, all species were optimized at the B3LYP/6-31 G (d)/RECP level in *n*DD to better predict their solvation energy[41]. This theory is based on the SMD universal continuum solvation model[42].

3 Results and discussion

Quantitative analysis of TODGA under different conditions after γ-ray irradiation

TODGA/*n*DD, HNO_3-TODGA/*n*DD, and neat TODGA were subjected to γ-irradiation with absorbed doses ranging from 20 to 500 kGy. The irradiated samples were measured quantitatively using HPLC-UV and their radiolytic stability was analyzed. Figure 1 shows that the TODGA concentration decreased exponentially with increasing absorbed doses, suggesting pseudo-first-order degradation kinetics for TODGA/*n*DD, HNO_3-TODGA/*n*DD, and neat TODGA. By comparing TODGA/*n*DD and HNO_3-TODGA/*n*DD, it was found that HNO_3 had little influence on the radiolysis of TODGA. Moreover, in the *n*DD solution, the radiolysis rate of TODGA was higher than that of the neat TODGA. A dodecane-induced "sensitization effect" is responsible for the sensitization of TODGA to radiolysis[43] due to the fact that the radiolysis of TODGA is accelerated by *n*DD solvents because of the efficiency of *n*DD in transferring positive charges [44–46].

Because the radiolysis behavior of TODGA depends on its concentration in pseudo-first-order kinetics, the rate of radiolysis causes an exponential drop in the TODGA concentration. The radiolysis rate equation is defined by Equation (2):

$$-\frac{dC_{TODGA}}{dR} = C_{TODGA} \cdot k \tag{2}$$

The solution to the rate equation is presented as Equation (3):

$$\frac{C_{TODGA}}{C^0_{TODGA}} = e^{-kR} \tag{3}$$

where C_{TODGA} (mol/L) is the concentration of TODGA, C^0_{TODGA} (mol/L) is the original concentration of TODGA before γ-radiation, R (kGy) is the absorbed dose, and the dose constant k (kGy^{-1}) is the coefficient obtained by fitting the exponential curve.

The dose constant k can be used to scale the absorbed dose when exponential behavior occurs[47]. Using all the information acquired during the irradiation experiment provides more accurate results, and standard statistical methods can be used to assess the accuracy of the results. The application of k to characterize an exponential curve in terms of the absorbed dose is very similar to that of traditional time-dependent kinetics. As expressed by exponential Equation (3), the reciprocal absorbed dose is governed by the first-order rate law instead of the reciprocal time.

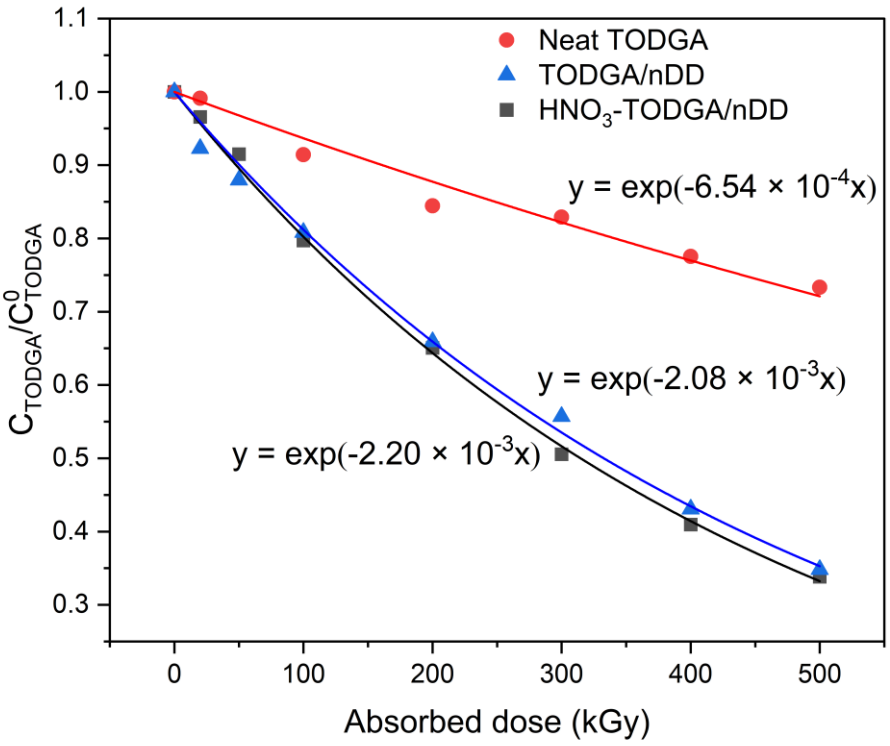

Figure 1 C_{TODGA}/C^0_{TODGA} of irradiated TODGA/*n*DD, HNO_3-TODGA/*n*DD, and neat TODGA as a function of the absorbed dose (R) (y: C_{TODGA}/C^0_{TODGA}, x: R)

If the dose constants k of different systems can be obtained, Equation (4) can be used to calculate the G value (μmol/J), which is known as the radiation chemical yield:

$$G = 10^3 C^0_{TODGA} k \rho^{-1} \quad (4)$$

where ρ is the solution density (kg/L) (ρ_{TODGA}= 0.91 and $\rho_{0.2\,mol/L\,TODGA/nDD}$= 0.77 (25 °C). The measurement results are shown in Table S1.

Table 1 shows the dose constants k and radiation chemical yields G of irradiated TODGA/*n*DD, HNO_3-TODGA/*n*DD, and neat TODGA. The dose constant k of TODGA in *n*DD is higher than that of neat TODGA because of the "sensitization effect," while the radiation chemical yields G of TODGA/*n*DD and HNO_3- TODGA/*n*DD are lower than that of neat TODGA because of the different initial concentrations of

irradiated TODGA. These results agree with the literature in which Sugo et al. reported that the k value of 0.2 mol/L TODGA/*n*DD was 2.2×10^{-3} kGy^{-1}[43, 48]. By using the k value, we can predict that the absorbed doses for the half-loss of TODGA concentration ($R_{0.5}$) in irradiated TODGA/*n*DD, HNO_3-TODGA/*n*DD, and neat TODGA will be approximately 330, 315, and 1060 kGy, respectively.

Table 1 Dose constants k, radiation chemical yields G, and absorbed dose for half-loss of concentration of TODGA $R_{0.5}$ of irradiated TODGA/*n*DD, HNO_3-TODGA/*n*DD, and neat TODGA

Samples	C^0_{TODGA} (mol/L)	k (kGy^{-1})	G (μmol/J)	$R_{0.5}$ (kGy)
TODGA/*n*DD	0.20	$(2.08\pm0.05)\times10^{-3}$	0.54±0.013	330
HNO_3-TODGA/*n*DD	0.20	$(2.20\pm0.03)\times10^{-3}$	0.57±0.008	315
Neat TODGA	1.57	$(6.54\pm0.31)\times10^{-4}$	1.13±0.053	1060

Identification and semi-quantitative analysis of radiolytic products

Ultra-high-performance liquid chromatography with quadrupole time-of-flight mass spectrometry (UPLC-QTOF-MS) can be used to identify and quantify complex mixtures of unknown compounds owing to its high resolution and mass accuracy.

The major radiolytic products of TODGA were identified using QTOF-MS; these are presented in Table 2, and their UPLC-QTOF-MS spectra are shown in Figures S3–9. Seven mass signals were identified and attributed to the possible radiolytic products of TODGA (P_1 – P_7, Table 2). These radiolytic products were formed by the rupture of the C – N, C – O, and C – C bonds of TODGA. Four radiolysis routes after irradiation are shown in Scheme 1.

Table 2 Radiolytic products of TODGA determined by the QTOF-MS

Radiolytic products	Chemical formula	Theoretical neutral mass	Observed neutral mass	Structure
P_1	$C_{28}H_{56}N_2O_3$	468.4291	468.4274	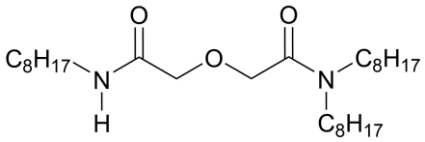
P_2	$C_{20}H_{39}NO_4$	357.2879	357.2892	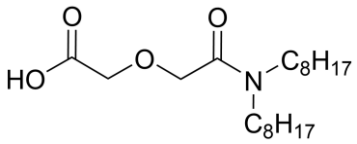
P_3	$C_{18}H_{37}NO_2$	299.2824	299.2825	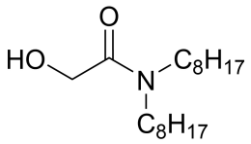
P_4	$C_{18}H_{37}NO$	283.2875	283.2867	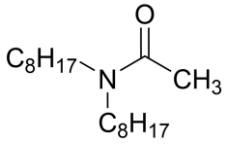
P_5	$C_{17}H_{35}NO$	269.2719	269.2719	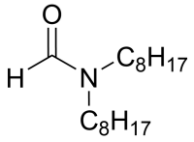
P_6	$C_{16}H_{35}N$	241.2770	241.2772	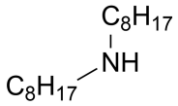
P_7	$C_{19}H_{39}NO_2$	313.2981	313.2994	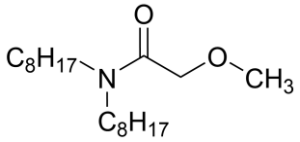

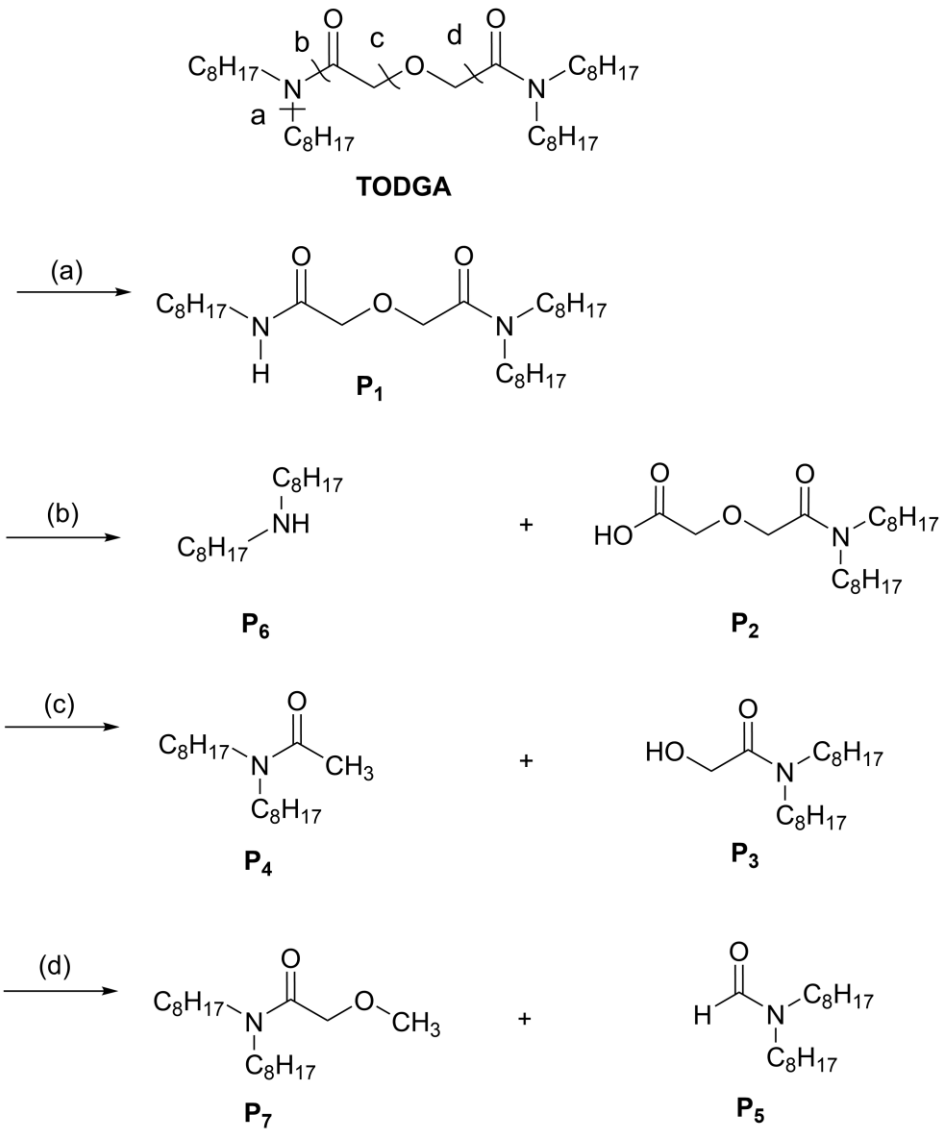

Scheme 1 Radiolysis routes of TODGA after γ-irradiation

Figure 2 shows the semi-quantitative analysis of the radiolytic products P_1 – P_7 in the irradiated HNO_3-TODGA/*n*DD and neat TODGA. The absorbed doses ranged from 20 to 500 kGy. Seven radiolytic products were found to exist in the two systems. The detector counts of the radiolytic products P_1 – P_7 roughly increased with increasing absorbed dose. However, some radiolytic products, such as P_1 in irradiated neat TODGA, showed a decrease in detector counts with absorbed doses from 400 kGy to 500 kGy. This is probably because the contents of the radiolytic products during irradiation increased from the radiolysis of the TODGA and decreased by self-radiolysis.

The concentration's rate of increase was less than the rate of decrease with absorbed doses from 400 to 500 kGy for P_1 in irradiated neat TODGA. The detector counts of all radiolytic products in irradiated TODGA/*n*DD were higher than those in neat TODGA (Figure S10), indicating the "sensitization effect" of *n*DD. This agreed well with the above result of the radiolysis kinetics of the TODGA with or without *n*DD. However, the relative detector counts of some radiolytic products differed between the two irradiation systems. For example, the detector count of P_6 was less than that of P_4 in irradiated neat TODGA; however, the converse was true for irradiated HNO_3-TODGA/*n*DD. This can be attributed to the different reaction mechanisms, wherein irradiated neat TODGA produces radical cations by direct ionization reaction. Conversely, in irradiated TODGA/*n*DD, *n*DD radical cations may transfer their charge to TODGA molecules, leading to radiolysis of TODGA[43, 49].

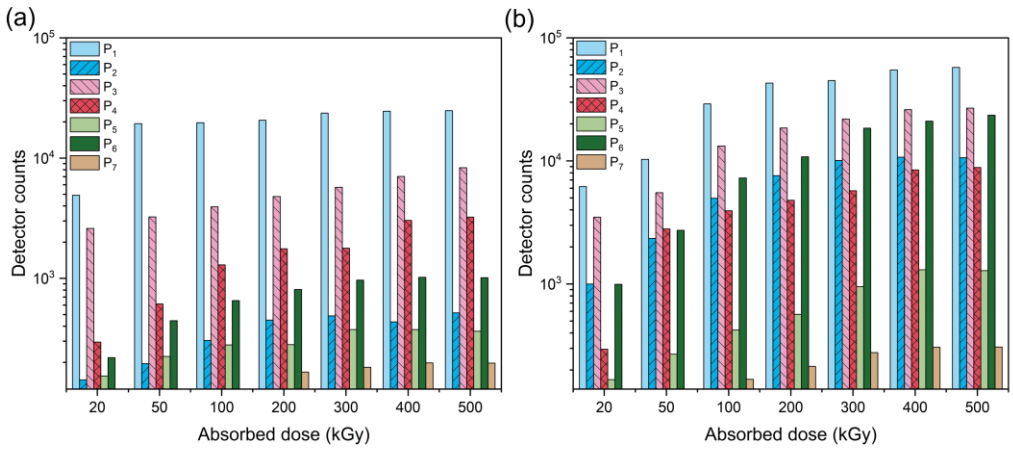

Figure 2 Semi-quantitative analysis of radiolytic products P_1 – P_7 in: (a) irradiated neat TODGA, and (b) HNO_3-TODGA/*n*DD with absorbed doses ranging from 20 to 500 kGy

Influence of γ-ray irradiation on the extraction of TODGA system toward Eu(III)

HNO_3-TODGA/*n*DD and neat TODGA were subjected to γ-ray irradiation at absorbed doses ranging from 50 to 500 kGy. The irradiated neat TODGA was diluted with *n*DD to 0.2 mol/L. These organic phases were used to extract Eu(III) from the 3.0 mol/L HNO_3 aqueous phase to evaluate the extraction performance.

As shown in Figure 3, D_{Eu} decreased as the absorbed dose increased, but it was slower for irradiated TODGA than for irradiated HNO_3-TODGA/*n*DD, indicating that γ-ray irradiation of the ligand significantly affected the extraction of Eu(III). This further proves that the presence of *n*DD increased the radiolysis of TODGA. However, the HNO_3-TODGA/*n*DD system after γ-ray irradiation still possesses a high D_{Eu} (2.2×10^3), even at 500 kGy.

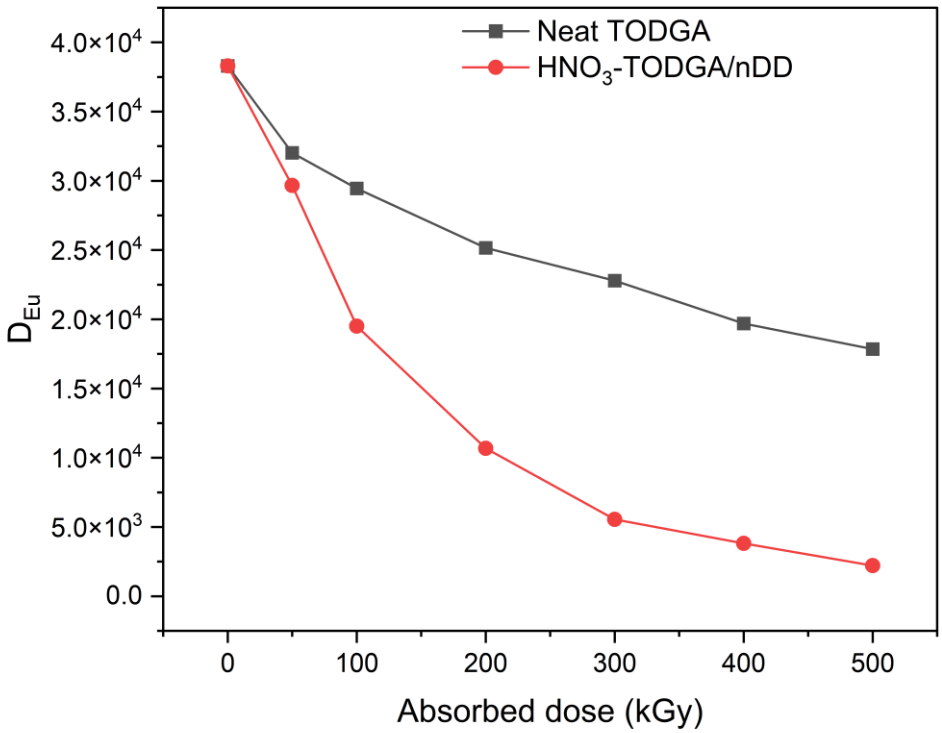

Figure 3 D_{Eu} of irradiated neat TODGA and HNO_3-TODGA/*n*DD for extraction of Eu(III) versus the absorbed dose.

The loss of extractants was the main cause of the decline in extractability after irradiation. Owing to the presence of TODGA and its liquid radiolysis products in the irradiated organic extraction phase, the complexation of radiolytic products on Eu(III) was studied using DFT calculations. This determined the effect if any of the radiolytic products of TODGA on the extraction behavior of the irradiated extraction system.

Slope analysis and fluorescence titration

Before DFT calculations were conducted to investigate the complexation of TODGA and its radiolytic products with Eu(III), we assessed the stoichiometry of Eu ions and TODGA ligands in the extraction reaction, which could be obtained by the slope analysis in the curve of $\log D_M - \log[L]_{(org.)}$.

The extraction reaction of Eu(III) by TODGA is expressed by Equation (5):

$$Eu^{3+}_{(aq.)} + 3NO^{-}_{3(aq.)} + nTODGA_{(org.)} \rightleftharpoons Eu(NO_3)_3TODGA_{n(org.)} \quad (5)$$

The extraction equilibrium concentration constant, K_{ex}, is described as Equation (6):

$$K_{ex} = \frac{[Eu(NO_3)_3TODGA_n]_{(org.)}}{[Eu^{3+}]_{(aq.)}[NO_3^-]^3_{(aq.)}[TODGA]^n_{(org.)}} \quad (6)$$

The distribution ratio, D_{Eu}, is defined as Equation (7):

$$D_{Eu} = \frac{[Eu(NO_3)_3TODGA_n]_{(org.)}}{[Eu^{3+}]_{(aq.)}} \quad (7)$$

Equation (7) was substituted into Equation (6), and Equation (6) was then transformed into a logarithmic form to obtain Equation (8).

$$\log D_{Eu} = \log K_{ex} + n\log[TODGA]_{(org.)} + 3\log[NO_3^-]_{(aq.)} \quad (8)$$

The n value can be calculated from Equation (8), which represents the average number of TODGA coordinated to one metal ion. The plot in Figure 4 of $\log D_{Eu} - \log[TODGA]_{(org.)}$ at a constant aqueous solution of 3.0 mol/L HNO_3 shows that the

slope is 3.10 ± 0.11, which indicates that Eu(III) would form complexes with three TODGA molecules.

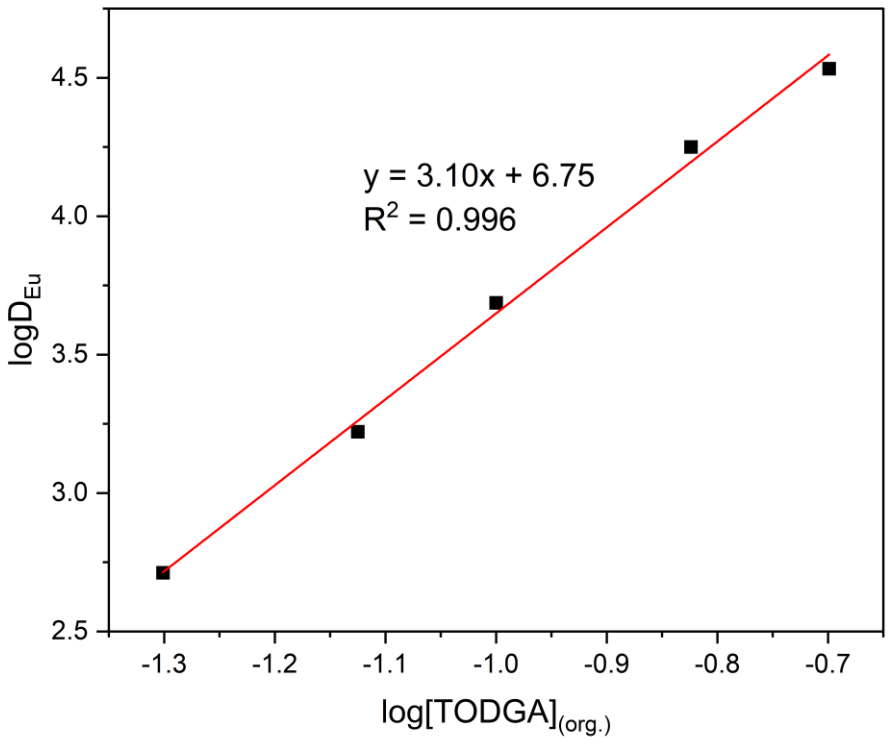

Figure 4 Plot of $\log D_{Eu}$ versus $\log[TODGA]_{(org.)}$ at a constant aqueous 3.0 mol/L HNO_3 solution (x: $\log[TODGA]_{(org.)}$, y: $\log D_{Eu}$)

Complexation studies were also performed with TODGA and Eu(III) using fluorescence titration. Figure 5 displays the normalized fluorescence emission spectra with different ratios of Eu(III) and TODGA resulting from the transitions of $5D_0 \rightarrow 7F_1$ and $5D_0 \rightarrow 7F_2$. The transition of $5D_0 \rightarrow 7F_1$ at 593 nm, owing to the magnetic-dipole transition, was considered independent of the ligand field. The transition of $5D_0 \rightarrow 7F_2$ at 617 nm owing to the electric–dipole transition is considered to be hypersensitive to the ligand field, and its intensity depends on the coordination symmetry around the metal ions[50]. With the addition of the TODGA ligand, the change in the ligand field led to a

gradual transformation of the single peak at 617 nm into a double peak, which was finally formed at M: L = 1:3. This indicated that the inner coordination sphere of Eu(III) was gradually occupied by TODGA with the addition of the ligand, which is similar to some results from the literature[51, 52].

The spectra of each component were obtained from the fluorescence emission spectra (Figure 6). The $[Eu(TODGA)_n]^{3+}$ (n = 1 – 3) complexes and Eu(III) solvent species were also discovered. No complexes with TODGA values greater than or equal to 4 were found in the fluorescence emission spectra, proving that the ratio of Eu(III) to TODGA equals 1:3.

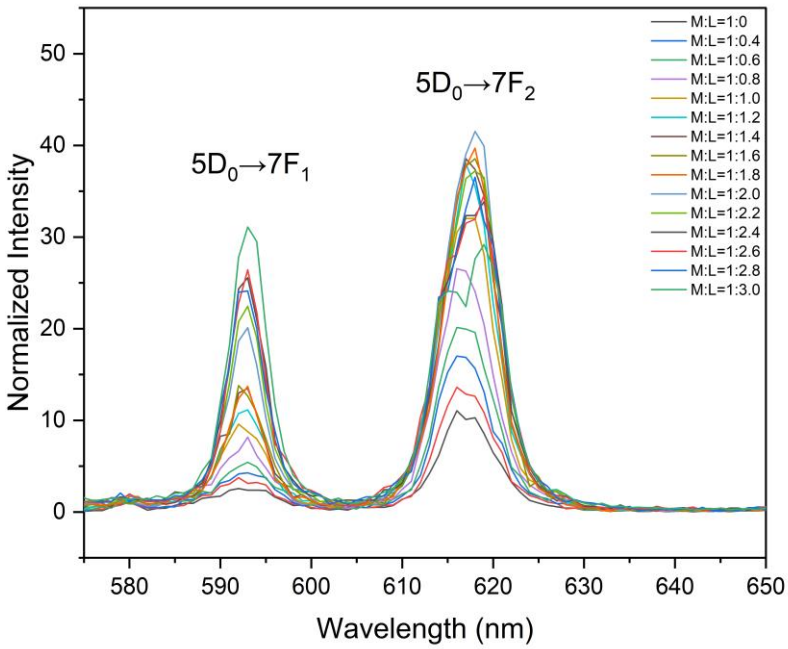

Figure 5 Normalized Eu(III) emission spectra as a result of the transitions of $5D_0 \rightarrow 7F_1$ and $5D_0 \rightarrow 7F_2$ for the complexation of Eu(III) with increasing TODGA in acetonitrile

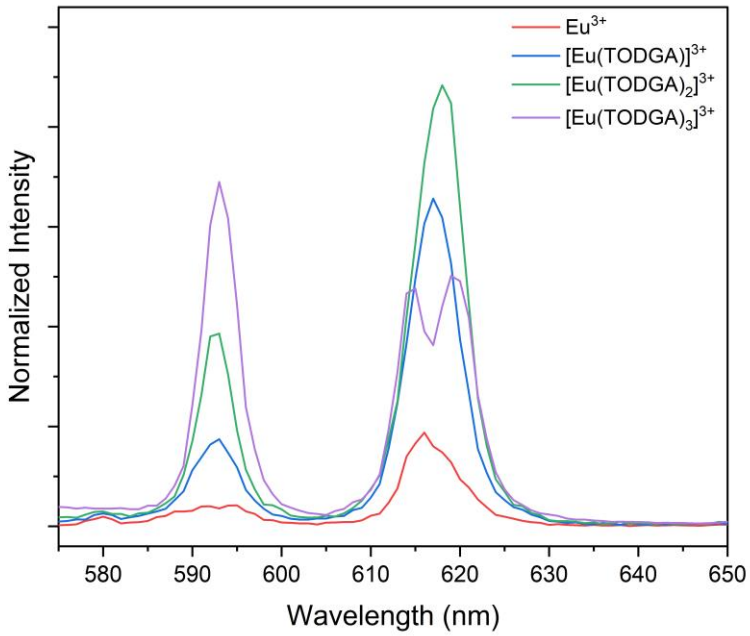

Figure 6 Single-component spectra of the $[Eu(TODGA)_n]^{3+}$ complexes (n = 1 – 3) and Eu(III) solvent species

The slope value was disputable, although many studies showed that the Ln(III): DGA structures are 1:3 complexes. Antonio et al. elucidated the inner coordination sphere of Eu(III) and TODGA using X-ray absorption spectroscopy (XAS)[53]. One ether O atom and two carbonyl O atoms of a TODGA molecule make up each ligand's tridentate to Eu(III). The coordination number is nine, with twelve distant carbon neighbors, six closest ones from carbonyl carbon atoms, and six slightly farther ones from the ether carbon atoms. Turanov et al.[54] found that the calculated slope value of Eu(III) extracted by TODGA in n-decane containing 0.002 mol/L dinonylnaphtalene sulfonic acid (HDNNS) was 3.28 ± 0.04. This was estimated by the plot of $\log D_{Eu}$ – $\log[TODGA]$ and the existence of $EuL_n(NO_3)_3$ species by the slope of $\log D_{Eu}$ – $\log[HNO_3]$, which was equal to 2.86 ± 0.08. Pathak et al.[55] investigated the influence of solvent type, acidity of extraction, and concentration of TODGA on luminescence lifetime and found that various ratios of TODGA to Eu ions resulted in the formation of

$Eu(TODGA)_3^{3+}$ species when Eu(III) was complexed with TODGA. According to the findings of Sasaki et al.[56], extracted Eu(III) complexes require three or four TODGA molecules and three nitrate ions to maintain stability in non-polar diluents by slope analysis. Zhu et al.[57] performed a slope analysis of TODGA to extract some Lns(III) and found that the slope was 3.9 for Eu(III), suggesting that the $M(TODGA)_4(NO_3)_3$ species finally formed. However, in this work, a 1:3 complexation ratio for TODGA with Eu(III) was determined.

The theoretical D_{Eu} values at different concentrations of TODGA can also be obtained using Equation (8). Equation (9) is obtained by linear fitting, as shown in Figure 4.

$$LogD_{Eu} = 3.10\ Log[TODGA]_{(org.)} + 6.75 \tag{9}$$

Equation (10) can be obtained from Figure 1 for irradiated HNO_3-TODGA/*n*DD. It is an exponential radiolysis equation for the concentration of TODGA and the absorbed dose.

$$\frac{C_{TODGA}}{C^0_{TODGA}} = e^{-2.20\times10^{-3}R} \tag{10}$$

We can obtain Equation (11) for D_{Eu} and the absorbed dose by substituting Equation (10) into Equation (9). This empirical equation enables us to construct a mathematical relationship between the D_{Eu} and absorbed dose in this system.

$$\log D_{Eu} = -2.965 \times 10^{-3}R + 4.583 \tag{11}$$

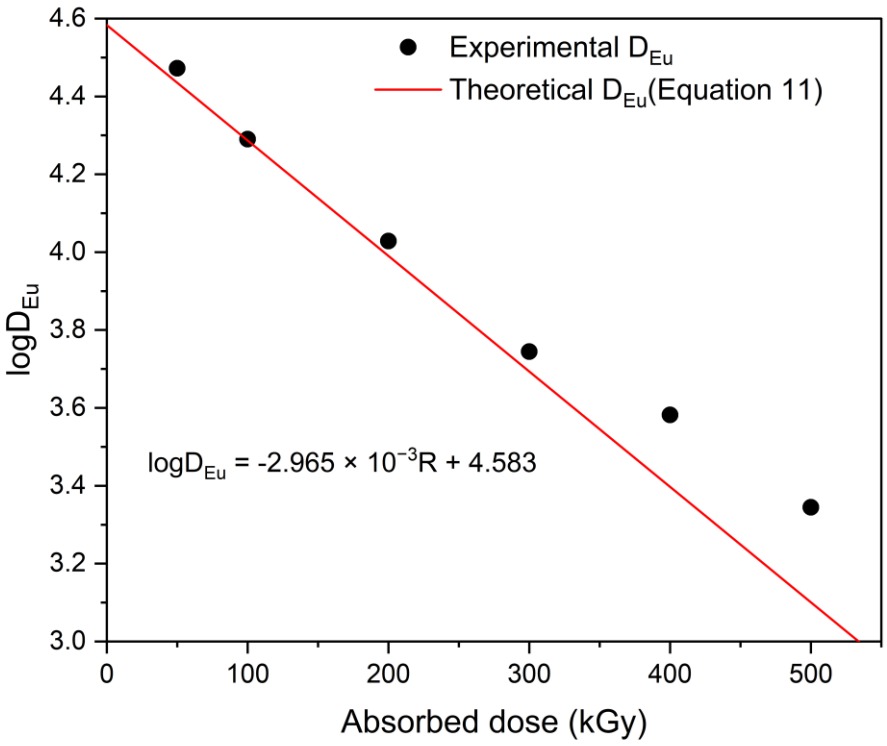

Figure 7 Experimental $\log D_{Eu}$ and theoretical $\log D_{Eu}$ after irradiation for HNO_3-TODGA/*n*DD

The theoretical D_{Eu} with absorbed doses ranging from 50 to 500 kGy was obtained using Equation (11). As shown in Figure 7, the experimental D_{Eu} was higher than the theoretical D_{Eu} after irradiation, particularly at a high absorbed dose above 300 kGy for the HNO_3-TODGA/*n*DD system. The experimental D_{Eu} is close to the theoretical D_{Eu} below 300 kGy, indicating that the decrease in D_{Eu} is mainly related to the loss of TODGA concentration, with a slight influence from radiolytic products.

Because some radiolytic products remained in coordination structures similar to those of TODGA, such as P_1 and P_2, which were identified by UPLC-QTOF, the complexation of radiolytic products on Eu(III) was investigated further using DFT calculations.

Theoretical calculations of complexation of TODGA and radiolytic products with Eu(III)

According to the slope and fluorescence titration analyses, the Eu(III): TODGA stoichiometry was 1:3. In addition, Kimberlin et al.[58] reported that several radiolytic products with the TODGA skeleton are involved in heteroleptic complexes with TODGA with a stoichiometry of 1:3 from the ESI-MS spectra. The time-resolved laser fluorescence results showed no change in the peak shape of the fluorescence spectra before and after irradiation (Figure S11). However, the fluorescence lifetime gradually decreased with increasing absorbed dose (Figure S12), indicating that γ radiation did not change the M: L ratio of 1:3 but caused a slight partial change in the original fluorescent species.

DFT calculations were employed to investigate the coordination abilities of TODGA and its radiolytic products with TODGA skeletons (P_1 and P_2). Figure 8 shows the optimized structures of the complexes formed by Eu(III) and the ligands. Theoretical calculations were performed for the $[Eu(TODGA)_2(P_n)]^{3+}$ (n = 1 – 2) species and $[Eu(TODGA)_3]^{3+}$ complexes. It is realistic that one TODGA molecule in the initial complex is replaced by one radiolytic product to form mixed Ln-radiolytic product-TODGA complexes during γ irradiation, which was already found in the ESI-MS spectra by Kimberlin et al.[58]. In addition, we investigated the optimized structures and coordination abilities of $[Eu(P_n)_3]^{3+}$ (n = 1 – 2), which were formed using three radiolytic products to represent a more extreme coordination environment of Eu(III) after γ irradiation.

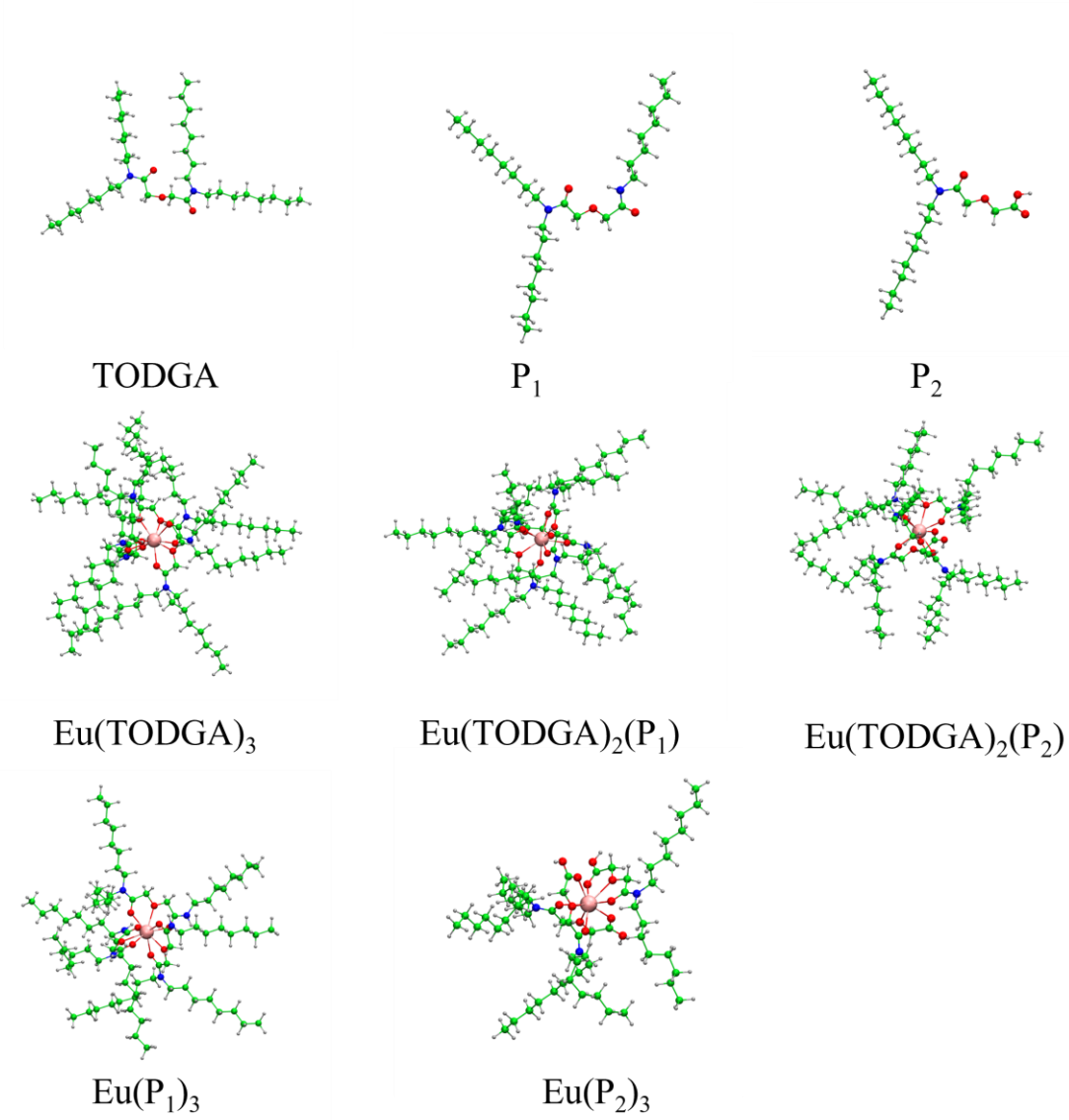

Figure 8 Optimized structures of the ligands (TODGA, P_1 and P_2) and complexes formed by Eu(III); the ligands (light pink, blue, green, red, and white spheres represent Eu(III), N, C, O, and H, respectively).

The changes in the Gibbs free energy, entropy, and enthalpy for the complexes formed by the ligands (TODGA, P_1 and P_2) and Eu(III) are shown in Table 3. It can be seen that the formation of $[Eu(TODGA)_3]^{3+}$ complex has more negative ΔG in the gas phase (-2527.3 kJ/mol) and in the *n*DD phase (-1115.0 kJ/mol) than that of the $[Eu(TODGA)_2(P_n)]^{3+}$ and $[Eu(P_n)_3]^{3+}$ (n = 1 – 2) complexes in the two phases. Moreover, the coordination abilities of the radiolytic products of TODGA decreased, as

reflected by the changes in the Eu–O bond length (Table 4). The average Eu – O bond length of the complexes changed from 2.4911 Å ($[Eu(TODGA)_3]^{3+}$) to 2.5000 Å ($[Eu(P_2)_3]^{3+}$), indicating a decline in the coordination ability of the complex. These results indicate that TODGA shows better coordination ability than the radiolytic products of TODGA; the complexation order is TODGA > P_1 > P_2. However, the formation of the $[Eu(TODGA)_2(P_n)]^{3+}$ and $[Eu(P_n)_3]^{3+}$ complexes (n = 1 – 2) had a high negative ΔG in the two phases. Theoretical calculations also indicated that the radiolytic products of TODGA, such as P_1 and P_2, still maintain a good coordination ability with Eu atoms, proving that the radiolytic products retain partial complexation for Eu(III). Consequently, the experimental D_{Eu} of TODGA was higher than the theoretical D_{Eu} from the loss of TODGA with the increase in radiolytic products at a high absorbed dose. Furthermore, if the contents of P_1 and P_2 are determined exactly, by combining the TODGA contents, we can predict the D_{Eu} of the irradiated TODGA/*n*DD system more precisely. This study will be conducted in future works. In our previous experiments, we found that the radiolytic products P_1 and P_2 were difficult to synthesize, and the radiolytic product P_1 was not sufficiently stable. Therefore, we used DFT calculations to evaluate the coordination abilities of these radiolytic products, thereby justifying the experimental result that the experimental D_{Eu} was higher than the theoretical D_{Eu} due to the high dose TODGA losses in this study.

Table 3 Changes in Gibbs free energy, entropy, and enthalpy (298.15 K, kJ/mol) for the complexes formed by ligands (TODGA, P_1 and P_2) and Eu(III) were acquired separately in (a) gas phase, as well as (b) *n*DD at the level of B3LYP/6-31G(d)/RECP.

(a) Complexation in the gas phase	ΔH_g	ΔG_g	$T\Delta S_g$
Eu^{3+} + 3TODGA → $[Eu(TODGA)_3]^{3+}$	-2693.7	-2527.3	-166.4
Eu^{3+} + 2TODGA+ P_1 → $[Eu(TODGA)_2(P_1)]^{3+}$	-2681.7	-2506.1	-175.6
Eu^{3+} + 2TODGA+ P_2 → $[Eu(TODGA)_2(P_2)]^{3+}$	-2657.8	-2487.8	-170.0
Eu^{3+} + 3P_1 → $[Eu(P_1)_3]^{3+}$	-2674.4	-2462.8	-211.6
Eu^{3+} + 3P_2 → $[Eu(P_2)_3]^{3+}$	-2568.0	-2380.8	-187.2
(b) Complexation in the *n*DD phase	ΔH_{sol}	ΔG_{sol}	$T\Delta S_{sol}$
Eu^{3+} + 3TODGA → $[Eu(TODGA)_3]^{3+}$	-1281.3	-1115.0	-166.3
Eu^{3+} + 2TODGA+ P_1 → $[Eu(TODGA)_2(P_1)]^{3+}$	-1276.4	-1100.9	-175.5
Eu^{3+} + 2TODGA+ P_2 → $[Eu(TODGA)_2(P_2)]^{3+}$	-1265.4	-1095.4	-170.0
Eu^{3+} + 3P_1 → $[Eu(P_1)_3]^{3+}$	-1282.1	-1070.5	-211.6
Eu^{3+} + 3P_2 → $[Eu(P_2)_3]^{3+}$	-1226.4	-1039.2	-187.2

Table 4 Changes in Eu – O bond length of complexes formed by Eu(III) and ligands (unit: Å)

Structure	Eu-O	Eu-O	Eu-O	Eu-O	Eu-O	Eu-O	Eu-O	Eu-O	Eu-O	Average
$[Eu(TODGA)_3]^{3+}$	2.4284	2.4293	2.4306	2.4325	2.436	2.439	2.6022	2.6088	2.6131	2.4911
$[Eu(TODGA)_2(P_1)]^{3+}$	2.4219	2.4222	2.4266	2.4306	2.4363	2.4532	2.6024	2.6111	2.6270	2.4924
$[Eu(TODGA)_2(P_2)]^{3+}$	2.3868	2.4142	2.4147	2.4215	2.4237	2.5415	2.5813	2.5957	2.6879	2.4964
$[Eu(P_1)_3]^{3+}$	2.4187	2.4217	2.4270	2.4371	2.4381	2.4408	2.6138	2.6146	2.6213	2.4926
$[Eu(P_2)_3]^{3+}$	2.3628	2.3821	2.3931	2.4798	2.4799	2.5147	2.6043	2.6271	2.6559	2.5000

In conclusion, by combining the exponential equation for the radiolysis kinetics of TODGA in *n*DD and the equation for slope analysis of the concentration of TODGA and D_{Eu}, we can derive a mathematical equation that includes the absorbed dose and D_{Eu}, which could be used to predict the extraction performance at low absorbed doses. This method can be used to study other extractant systems. This work provides in-depth

insights into the effect of γ irradiation on the extraction behavior of the TODGA/*n*DD system and provides useful information on the use of nuclear fuel reprocessing.

4 Conclusions

In summary, γ-radiolysis of TODGA/*n*DD and HNO_3-TODGA/*n*DD was investigated and compared with γ-radiolysis of neat TODGA by analyzing the loss of TODGA and liquid radiolytic products. When the absorbed dose was increased, the TODGA concentration decreased exponentially, and the dose constant of TODGA in *n*DD was higher than that of neat TODGA because of the "sensitization effect" of *n*DD. However, the radiolysis of TODGA in *n*DD was only slightly affected by the pre-equilibration with HNO_3. Seven radiolytic products of TODGA were identified and semi-quantified using UPLC-QTOF-MS, and four radiolysis routes for TODGA were proposed. The D_{Eu} of the irradiated systems decreased after irradiation, but the HNO_3-TODGA/*n*DD system irradiated with an absorbed dose of 500 kGy maintained a high D_{Eu} of 2.2×10^3. For the irradiated HNO_3-TODGA/*n*DD, we obtained an empirical equation between D_{Eu} and the absorbed dose by combining the radiolysis kinetics of TODGA and the complexation equation of TODGA with Eu(III), which fits well with the experimental results with absorbed doses below 300 kGy. DFT calculations demonstrated that the radiolytic products of TODGA with similar coordination structures possessed good coordination abilities with Eu atoms, which led to the experimental D_{Eu} being higher than the theoretical D_{Eu} based on the ligand content at high absorbed doses.

Acknowledgments: The measurements of UPLC-QTOF and ICP-MS were performed at the Analytical Instrumentation Center of Peking University. We acknowledge the help from PKUAIC (Dr. Jiang Zhou, Dr. Li Zhang, and Dr. Jia-Hui Liu). The authors

also wish to acknowledge Prof. Song-Dong Ding (Sichuan University) for his assistance in providing TODGA.

References

1. S.A. Ansari, P.K. Mohapatra, A review on solid phase extraction of actinides and lanthanides with amide based extractants. J. Chromatogr. A. 1499, 1–20 (2017). https://doi.org/10.1016/j.chroma.2017.03.035

2. S.A. Ansari, P. Pathak, P.K. Mohapatra et al., Chemistry of Diglycolamides: Promising Extractants for Actinide Partitioning. Chem. Rev. 112, 1751–1772 (2012). https://doi.org/10.1021/cr200002f

3. M. Salvatores, G. Palmiotti, Radioactive waste partitioning and transmutation within advanced fuel cycles: Achievements and challenges. Prog. Part. Nucl. Phys. 66, 144–166 (2011). https://doi.org/10.1016/j.ppnp.2010.10.001

4. L. Rodríguez-Penalonga, B. Moratilla Soria, A Review of the Nuclear Fuel Cycle Strategies and the Spent Nuclear Fuel Management Technologies. Energies. 10, 1235 (2017). https://doi.org/10.3390/en10081235

5. X.L. Liu, G. Verma, Z.S. Chen et al., Metal-organic framework nanocrystal-derived hollow porous materials: Synthetic strategies and emerging applications. The Innovation. 3, 100281 (2022). https://doi.org/10.1016/j.xinn.2022.100281

6. Y.F. Zhang, H.X. Liu, F.X. Gao et al., Application of MOFs and COFs for photocatalysis in CO_2 reduction, H_2 generation, and environmental treatment. EnergyChem. 4, 100078 (2022). https://doi.org/10.1016/j.enchem.2022.100078

7. X. Wang, S.Q. Pan, Q.K. Zhao et al., The status of ITER radioactive waste management and enlightenment to CFETR radioactive waste management. Nucl. Tech. 45, 090603 (2022). https://doi.org/10.11889/j.0253-3219.2022.hjs.45.090603 (in Chinese)

8. L.Y. Zhen, J.J. Zhang, Y.H. Lin et al., Analysis of the accuracy of ^{14}C in gaseous effluent of nuclear power plant by direct measurement method. Nucl. Tech. 45, 090301 (2022). https://doi.org/10.11889/j.0253-3219.2022.hjs.45.090301 (in Chinese)

9. G. Yang, J.R. Lin, X.Y. Yang et al., Adsorption properties of surrounding rock for ^{137}Cs in a cavern-type low and intermediate radioactive waste repository. Nucl. Tech. 45, 080301 (2022). https://doi.org/10.11889/j.0253-3219.2022.hjs.45.080301 (in Chinese)

10. S.Q. Meng, Y.S. Hu, T.M. Ruan, Impact of nickel and iron on PWR zirconium alloy surface CRUD formation and boron precipitation. Nucl. Tech. 45, 060602 (2022). https://doi.org/10.11889/j.0253-3219.2022.hjs.45.060602 (in Chinese)

11. M. Nilsson, K.L. Nash, Review Article: A Review of the Development and Operational Characteristics of the TALSPEAK Process. Solvent Extr. Ion Exch. 25, 665–701 (2007). https://doi.org/10.1080/07366290701634636

12. W.H. Duan, T.X. Sun, J.C. Wang, An industrial-scale annular centrifugal extractor for the TRPO process. Nucl. Sci. Tech. 29, 46 (2018). https://doi.org/10.1007/s41365-018-0395-z

13. Y. Sugo, Y. Sasaki, S. Tachimori, Studies on hydrolysis and radiolysis of N, N, N', N'-tetraoctyl-3-oxapentane-1,5-diamide. Radiochim. Acta. 90, 161–165 (2002). https://doi.org/10.1524/ract.2002.90.3_2002.161

14. D. Whittaker, A. Geist, G. Modolo et al., Applications of Diglycolamide Based Solvent Extraction Processes in Spent Nuclear Fuel Reprocessing, Part 1: TODGA. Solvent Extr. Ion Exch. 36, 223–256 (2018). https://doi.org/10.1080/07366299.2018.1464269

15. Z. Dong, W.J. Yuan, C. Liu et al., Th(IV) and U(VI) removal by TODGA in ionic liquids: extraction behavior and mechanism, and radiation effect. Nucl. Sci. Tech. 28, 62 (2017). https://doi.org/10.1007/s41365-017-0214-y

16. A. Geist, U. Müllich, D. Magnusson et al., Actinide(III)/Lanthanide(III) Separation Via Selective Aqueous Complexation of Actinides(III) using a Hydrophilic 2,6-Bis(1,2,4-Triazin-3-Yl)-Pyridine in Nitric Acid. Solvent Extr. Ion Exch. 30, 433–444 (2012). https://doi.org/10.1080/07366299.2012.671111

17. P.K. Nayak, R. Kumaresan, K.A. Venkatesan et al., Extraction Behavior of Am(III) and Eu(III) from Nitric Acid Medium in Tetraoctyldiglycolamide-Bis(2-Ethylhexyl)Phosphoric Acid Solution. Sep. Sci. Technol. 49, 1186–1191 (2014). https://doi.org/10.1080/01496395.2013.874357

18. M.B. Singh, S.R. Patil, A.A. Lohi et al., Insight into nitric acid extraction and aggregation of N, N, N', N'-Tetraoctyl diglycolamide (TODGA) in organic solutions by molecular dynamics simulation. Sep. Sci. Technol. 53, 1361–1371 (2018). https://doi.org/10.1080/01496395.2018.1445107

19. A. Wilden, G. Modolo, P. Kaufholz et al., Laboratory-Scale Counter-Current Centrifugal Contactor Demonstration of an Innovative-SANEX Process Using a Water Soluble BTP. Solvent Extr. Ion Exch. 33, 91–108 (2015). https://doi.org/10.1080/07366299.2014.952532

20. G. Modolo, A. Wilden, P. Kaufholz et al., Development and demonstration of innovative partitioning processes (i-SANEX and 1-cycle SANEX) for actinide partitioning. Prog. Nucl. Energ. 72, 107–114 (2014). https://doi.org/10.1016/j.pnucene.2013.07.021

21. J. Brown, F. McLachlan, M. Sarsfield et al., Plutonium Loading of Prospective Grouped Actinide Extraction (GANEX) Solvent Systems based on Diglycolamide

Extractants. Solvent Extr. Ion Exch. 30, 127–141 (2012). https://doi.org/10.1080/07366299.2011.609378

22. K. Bell, C. Carpentier, M. Carrott et al., Progress Towards the Development of a New GANEX Process. Procedia Chemistry. 7, 392–397 (2012). https://doi.org/10.1016/j.proche.2012.10.061

23. R. Malmbeck, D. Magnusson, S. Bourg et al., Homogenous recycling of transuranium elements from irradiated fast reactor fuel by the EURO-GANEX solvent extraction process. Radiochim. Acta. 107, 917–929 (2019). https://doi.org/10.1515/ract-2018-3089

24. I. Kajan, M. Florianová, C. Ekberg et al., Effect of diluent on the extraction of europium(III) and americium(III) with N, N, N', N'-tetraoctyl diglycolamide (TODGA). RSC Adv. 11, 36707–36718 (2021). https://doi.org/10.1039/D1RA07534A

25. S. Panja, P.K. Mohapatra, S.C. Tripathi et al., Role of organic diluents on Am(III) extraction and transport behaviour using N, N, N', N'-tetraoctyl-3-oxapentanediamide as the extractant. J. Membr. Sci. 403–404, 71–77 (2012). https://doi.org/10.1016/j.memsci.2012.02.022

26. J. Veliscek-Carolan, Separation of actinides from spent nuclear fuel: A review. J. Hazard. Mater. 318, 266–281 (2016). https://doi.org/10.1016/j.jhazmat.2016.07.027

27. Y. Wang, Y.Y. Ao, W.J. Yuan et al., Extraction performance of Eu^{3+} by using heterocyclic N-donor ligands with different structures in ionic liquids: an experimental and theoretical study. New J. Chem. 42, 7206–7212 (2018). https://doi.org/10.1039/C8NJ00517F

28. C. Marie, P. Kaufholz, V. Vanel et al., Development of a Selective Americium Separation Process Using H_4TPAEN as Water-Soluble Stripping Agent. Solvent Extr. Ion Exch. 37, 313–327 (2019). https://doi.org/10.1080/07366299.2019.1643569

29. Y. Wang, J. Peng, W. Huang et al., A new strategy for identifying the water-insoluble radiolytic products of BPC6/ionic liquids and accessing their influence on the Cs extraction. Radiat. Phys. Chem. 165, 108408 (2019). https://doi.org/10.1016/j.radphyschem.2019.108408

30. C.A. Zarzana, G.S. Groenewold, B.J. Mincher et al., A Comparison of the γ - Radiolysis of TODGA and T(EH)DGA Using UHPLC-ESI-MS Analysis. Solvent Extr. Ion Exch. 33, 431–447 (2015). https://doi.org/10.1080/07366299.2015.1012885

31. P. Zsabka, K. Van Hecke, A. Wilden et al., Gamma radiolysis of TODGA and CyMe$_4$BTPhen in the ionic liquid tri-n-octylmethylammonium nitrate. Solvent Extr. Ion Exch. 38, 212–235 (2020). https://doi.org/10.1080/07366299.2019.1710918

32. Y. Sugo, M. Taguchi, Y. Sasaki et al., Radiolysis study of actinide complexing agent by irradiation with helium ion beam. Radiat. Phys. Chem. 78, 1140–1144 (2009). https://doi.org/10.1016/j.radphyschem.2009.06.031

33. W.T. Xu, Y.F. Zhou, D.C. Huang et al., Luminescent sensing profiles based on anion- responsive lanthanide(III) quinolinecarboxylate materials: solid-state structures, photophysical properties, and anionic species recognition. J. Mater. Chem. C. 3, 2003–2015 (2015). https://doi.org/10.1039/C4TC02369B

34. C. Lee, W. Yang, R.G. Parr, Development of the Colle-Salvetti correlation-energy formula into a functional of the electron density. Phys. Rev. B. 37, 785–789 (1988). https://doi.org/10.1103/PhysRevB.37.785

35. A.D. Becke, Density-functional thermochemistry. III. The role of exact exchange. J. Chem. Phys. 98, 5648–5652 (1993). https://doi.org/10.1063/1.464913

36. W. Küchle, M. Dolg, H. Stoll et al., Energy-adjusted pseudopotentials for the actinides. Parameter sets and test calculations for thorium and thorium monoxide. J. Chem. Phys. 100, 7535–7542 (1994). https://doi.org/10.1063/1.466847

37. X. Cao, M. Dolg, Segmented contraction scheme for small-core actinide pseudopotential basis sets. J. Mol. Struct. 673, 203–209 (2004). https://doi.org/10.1016/j.theochem.2003.12.015

38. M. Dolg, H. Stoll, A. Savin et al., Energy-adjusted pseudopotentials for the rare earth elements. Theoret. Chim. Acta. 75, 173–194 (1989). https://doi.org/10.1007/BF00528565

39. M. Dolg, H. Stoll, H. Preuss, A combination of quasirelativistic pseudopotential and ligand field calculations for lanthanoid compounds. Theoret. Chim. Acta. 85, 441–450 (1993). https://doi.org/10.1007/BF01112983

40. M. Dolg, H. Stoll, H. Preuss, Energy-adjusted ab initio pseudopotentials for the rare earth elements. J. Chem. Phys. 90, 1730–1734 (1989). https://doi.org/10.1063/1.456066

41. H. Struebing, Z. Ganase, P.G. Karamertzanis et al., Computer-aided molecular design of solvents for accelerated reaction kinetics. Nature Chem. 5, 952–957 (2013). https://doi.org/10.1038/nchem.1755

42. A.V. Marenich, C.J. Cramer, D.G. Truhlar, Universal Solvation Model Based on Solute Electron Density and on a Continuum Model of the Solvent Defined by the Bulk Dielectric Constant and Atomic Surface Tensions. J. Phys. Chem. B. 113, 6378–6396 (2009). https://doi.org/10.1021/jp810292n

43. Y. Sugo, Y. Izumi, Y. Yoshida et al., Influence of diluent on radiolysis of amides in organic solution. Radiat. Phys. Chem. 76, 794–800 (2007). https://doi.org/10.1016/j.radphyschem.2006.05.008

44. H. Galán, A. Núñez, A.G. Espartero et al., Radiolytic Stability of TODGA: Characterization of Degraded Samples under Different Experimental Conditions. Procedia Chem. 7, 195–201 (2012). https://doi.org/10.1016/j.proche.2012.10.033

45. H. Galán, C.A. Zarzana, A. Wilden et al., Gamma-radiolytic stability of new methylated TODGA derivatives for minor actinide recycling. Dalton Trans. 44, 18049–18056 (2015). https://doi.org/10.1039/C5DT02484F

46. W.J. Yuan, C.Z. Wang, Y.Y. Ao et al., γ-Radiation effect on Th^{4+} extraction behaviour of TODGA/[C_2mim][NTf_2]: identification and extractability study of radiolytic products. RSC Adv. 6, 7626–7632 (2016). https://doi.org/10.1039/C5RA25364K

47. B.J. Mincher, R.D. Curry, Considerations for choice of a kinetic fig. of merit in process radiation chemistry for waste treatment. Appl. Radiat. Isot. 5 (2000). https://doi.org/10.1016/S0969-8043(99)00161-X

48. R. Malmbeck, N.L. Banik, Radiolytic behaviour of a TODGA based solvent under alpha irradiation. J. Radioanal. Nucl. Chem. 326, 1609–1615 (2020). https://doi.org/10.1007/s10967-020-07444-7

49. S.P. Mezyk, B.J. Mincher, S.B. Dhiman et al., The role of organic solvent radical cations in separations ligand degradation. J. Radioanal. Nucl. Chem. 307, 2445–2449 (2016). https://doi.org/10.1007/s10967-015-4582-7

50. B. Rajamouli, P. Sood, S. Giri et al., A Dual-Characteristic Bidentate Ligand for a Ternary Mononuclear Europium(III) Molecular Complex – Synthesis, Photophysical, Electrochemical, and Theoretical Study. Eur. J. Inorg. Chem. 2016, 3900–3911 (2016). https://doi.org/10.1002/ejic.201600508

51. A. Wilden, G. Modolo, S. Lange et al., Modified Diglycolamides for the An(III) + Ln(III) Co-separation: Evaluation by Solvent Extraction and Time-Resolved Laser Fluorescence Spectroscopy. Solvent Extr. Ion Exch. 32, 119–137 (2014). https://doi.org/10.1080/07366299.2013.833791

52. A. Sengupta, P.K. Mohapatra, M. Iqbal et al., Spectroscopic investigations of Eu^{3+}-complexes with ligands containing multiple diglycolamide pendant arms in a room temperature ionic liquid. J. Lumin. 154, 392–401 (2014). https://doi.org/10.1016/j.jlumin.2014.05.001

53. M.R. Antonio, D.R. McAlister, E.P. Horwitz, An europium(III) diglycolamide complex: insights into the coordination chemistry of lanthanides in solvent extraction. Dalton Trans. 44, 515–521 (2015). https://doi.org/10.1039/C4DT01775G

54. A.N. Turanov, V.K. Karandashev, Synergistic Extraction of U(VI), Th(IV), and Lanthanides(III) from Nitric Acid Solutions Using Mixtures of TODGA and Dinonylnaphthalene Sulfonic Acid. Solvent Extr. Ion Exch. 36, 257–271 (2018). https://doi.org/10.1080/07366299.2018.1459157

55. P.N. Pathak, S.A. Ansari, S.V. Godbole et al., Interaction of Eu^{3+} with N, N, N', N'-tetraoctyl diglycolamide: A time resolved luminescence spectroscopy study. Spectroc. Acta Pt. A-Molec. Biomolec. Spectr. 73, 348–352 (2009). https://doi.org/10.1016/j.saa.2009.02.040

56. Y. Sasaki, P. Rapold, M. Arisaka et al., An Additional Insight into the Correlation between the Distribution Ratios and the Aqueous Acidity of the TODGA System. Solvent Extr. Ion Exch. 25, 187–204 (2007). https://doi.org/10.1080/07366290601169345

57. Z.X. Zhu, Y. Sasaki, H. Suzuki et al., Cumulative study on solvent extraction of elements by N, N, N', N'-tetraoctyl-3-oxapentanediamide (TODGA) from nitric acid into n-dodecane. Anal. Chim. Acta. 527, 163–168 (2004). https://doi.org/10.1016/j.aca.2004.09.023

58. A. Kimberlin, D. Guillaumont, S. Arpigny et al., An experimental and computational look at the radiolytic degradation of TODGA and the effect on metal

complexation. New J. Chem. 45, 12479–12493 (2021).

https://doi.org/10.1039/D1NJ01143J